Thermally induced strain in joints with dissimilar adherends bonded with a flexible adhesive

Thermally induced strain in joints with dissimilar adherends bonded with a flexible adhesive

V.Bagiatis[a], G.W.Critchlow[a,*] D. Price[a], S.Wang[b], C.M.Harvey[b] and B.Yuan[b]

[a] Department of Materials, Loughborough University, Loughborough, LE12 3TU, UK

[b] Department of Aeronautical and Automotive Engineering, Loughborough University, Loughborough, LE12 3TU, UK

Corresponding author: g.w.critchlow@lboro.ac.uk

Abstract

In this study, assemblies comprising poly(methyl methacrylate) (PMMA) bonded to glass were subjected to a temperature gradient from +30°C to -40°C at 0% humidity. Their behaviour was recorded using a 3D digital image correlation (DIC) setup. The deformations and the thermally induced surface strain development, due to thermal loading, were recorded using a stereo camera system with two charge-coupled device (CCD) cameras. Narrow field measurements were performed near the edges of the joint where a high concentration of peeling and shear strains might be expected. With the use of commercial DIC software, the thermal deformation of the structure and the developed surface strain fields (ε_{xx}, γ_{xy}, ε_{yy}) are analysed. Joints with different bond line thickness (0.5 mm, 2 mm, 3.2 mm) of the silicone adhesive were investigated. The continuous image capture with the CCD cameras allowed identification of the failure conditions and the exact moment of failure of the bonded assembly. Additionally, the DIC experiment results were evaluated with the help of finite-element analysis results, which are in excellent agreement. This showed that the DIC method can be successfully applied for the investigation of thermally induced strains in adhesively bonded assemblies and thus contribute to understanding of the underlying thermal/mechanical behaviour of bonded systems.

Keywords: silicone; surface treatment; non-destructive testing; hybrid joints, and; digital image correlation.

1 Introduction

One of the main structural integrity issues in optical, photonic and microelectronic assemblies is their reliable performance under thermal cycling or prolonged exposure to extreme temperatures. Such conditions can occur during, for example: the manufacturing or testing stage; transportation, or; while in-service. Usually, these assemblies consist of multilayered structures of different materials with dissimilar coefficients of thermal expansion (CTE) which are typically adhesively bonded or soldered together [1]. In this case, each material in the assembly is subject to different expansion or contraction rates under an applied temperature gradient. These different expansion or contraction rates lead to the development of thermally induced strains and stresses that can cause: delamination; excess undesired bending ,or; fracture of the bonded assemblies [2–4]. More specifically, in adhesively bonded structures subject to low temperatures, cracking in the midportion of the low expansion layer might occur due to excessive bending of the assembly. In this case, the bending induced tensile stress exceeds the compressive stress from the thermal contraction mismatch of the assembly. Use of materials without highly dissimilar CTE values can reduce the excessive bending and overcome this type of failure. Cracks in the corners of the substrates or possible delamination can be attributed to elevated interfacial shearing and peeling stresses which have their maximum values towards the edges of the bonded assemblies. These types of failures can be avoided with the use of thicker bondlines or with low modulus, flexible adhesives [5]. To illustrate this, Figure 1, from the present study, shows a combination of the previously mentioned failure modes in a PMMAglass assembly bonded with a high modulus ultra violet radiation curable adhesive which was subjected to low temperature isothermal exposure at -40ºC. In this case, there is a crack in the midportion of the low CTE layer (glass) and also cracks in the corners due to high concentration of shearing and peeling stresses.

Figure 1: Failure in a PMMA-glass bonded assembly subjected to low temperature (-40ºC) exposure when bonded with high modulus UV curable adhesive. Note the cracks in the middle and the corners of the upper glass layer

These issues are often experienced in the development of photonics or optical assemblies where highly dissimilar materials such as glass and polymers are being employed. Typically, optical cements, cyanoacrylates, UV curable adhesives and transparent elastomers are used in the manufacture of these bonded assemblies. Although high modulus adhesives such as optical cements and cyanoacrylates can provide very rigid bonds, they cannot efficiently accommodate the thermally induced stresses due to the CTE mismatch of the adherents [6]. In contrast, flexible UV curable acrylate adhesives can overcome this problem but such adhesives can often be susceptible to yellowing after prolonged light exposure, a fact that prevents them from being suitable candidate adhesives in applications that require high transparency and clear bondlines [7,8]. Low modulus elastomers, and more specifically optically transparent silicones, can overcome the two aforementioned problems but because they cannot form very strong bonds, especially with polymers [9], they are prone to delamination failures. In order to eliminate this kind of failure, improvement of the adhesion on these surfaces can be achieved with the use of appropriate surface pretreatment methods [10]. The use of high Young's modulus adhesives in the middle of assemblies with low modulus adhesives at the edges has also been examined [11], although such an approach in the development of assemblies where excellent transparency and uniform layers are required, makes this problematic. To avoid unexpected failures in optical devices incorporating CTE mismatched materials, extended investigation and testing are required during the design and product development and in the manufacturing and qualification stages.

Analytical work on the development of thermal stresses in multimaterial layered structures when subjected to temperature loading has been made by Taylor and Yuan [12] following the theory of Volkersen [13]. In addition, Chen and Nelson [14], Suhir [15–17], Jiang et al. [18] and more recently Wong et al. [19] and He [20] have developed analytical models describing thermal deformations and interfacial stresses caused by CTE mismatch in bonded joints. Despite their high importance, analytical models can be highly complex and as a result the finite-element analysis (FEA)

approach is widely used today in the design and stress-strain evaluations of optical and microelectronics assemblies. Aiming to evaluate the results of FEA models and improve their accuracy, a variety of experimental methods can be used to capture the displacement and stress and strain distribution in bonded joints. Moreover, these experimental methods can be employed in the investigation of the behaviour of bonded assemblies of complex geometry or when there is absence of the materials' properties data. Such methods include: thermoelastic stress analysis; Moiré interferometry, and; digital image correlation (DIC). The latter of these, DIC, has gained in popularity in recent years due to its: accuracy; ease of use; limited requirement for sample preparation; cost effectiveness, and; its capacity to be used in a wide range of potential applications.

DIC is gaining attention in the field of adhesion science and technology, currently being utilised in the inspection of bonded joints under mechanical loading. For example, Moutrille et al. assessed, with the use of DIC, the shear strain field in an adhesive joint between composites and aluminium. In this study, Moutrille et al demonstrated the effectiveness of DIC, in comparison with numerical and analytical results, as a technique to effectively determine the displacement field and strain distribution through the thickness of the adhesive [21]. Kashfuddoja et al monitored the displacement and the strain distribution through the thickness in single sided CFRP patch repair configurations using DIC, and found a good agreement with the results predicted by FEA [22]. DIC strain monitoring through the thickness of thick adherends bonded with epoxy film adhesives was conducted in the study of Kosmann et al. The comparison with the numerical results proved that DIC can provide reliable engineering data [23]. Naik et al. used DIC in a comparative study with FEA to investigate the joint behaviour in single and dual adhesive bonds between the CFRP and aluminium adherends [24]. Bamberg et al. [25] also employed DIC in dissimilar and similar adherends in order to study the effects of the overlap length, adhesive thickness and the adherends yield strength [25]. The DIC method was used by Caminero et al. [26] to investigate the damage and performance of adhesively bonded patch repairs in composite panels under tensile loading, successfully measuring the surface strains and relating them to possible damage mechanisms that could occur in the composite system. Their experimental results were in good agreement with those obtained with the analytical predictions. Aiming to investigate the bending moments in adhesively bonded single lap joints with

epoxies, Silva et al. [27] used DIC in comparison with theoretical results and found good agreement with advanced analytical predictions. A combination of optical measurement with DIC and FEA analysis was proposed by Bai et al. [28] to obtain the stress distribution at the adhesive layer in a composite single-lap adhesively bonded joint with errors of <1%.

Comparative studies with DIC and other techniques have also been conducted. For example, in a combined study with thermoelastic stress analysis and DIC, by Crammond et al. [29], These workers investigated the stress and strain distributions in bonded composite joints, achieving a good agreement between the two experimental methods[29]. In addition, Zarouchas et al. [30] utilised DIC in order to inspect the static mechanical properties of thick adhesives used in wind industry in combination with the acoustic emission technique.

The use of DIC for the inspection of joined assemblies under thermal loading has mainly focused on soldered joints in electronics packaging and assembly. In the study of Kwak et al. [31] DIC was used to capture the thermo-mechanical behaviour of soldered joints, obtaining the deformations and strain development in a temperature range between 25 °C to 100°C. Tominaga et al. [32] observed the thermally induced strain development between 30 °C to 230°C in bi-metal assemblies via DIC, aiming to establish a measurement system of thermal deformations in electronic packages. Aiming to investigate the thermal deformation of a BGA package made of materials with varying coefficients of thermal expansion, Zhang et al. [33] used DIC to obtain the developed strain fields from 30 °C to 150°C.

Of direct relevance to the present study, DIC for the inspection of bonded assemblies under a temperature gradient is currently limited in a small number of studies. Deheeger et al. [34] assessed the thermal stress distribution in a composite/aluminium bonded joint with the use of DIC, examining the displacement and strain distribution on the side of a composite patch in a temperature range between 20 °C to 110°C. In addition, DIC was used to investigate the thermomechanical deformations in a laminated assembly joined with a flexible EVA sheet simulating a PV module under a temperature gradient by Einer et al. [35]. In their study they also examined possible measurement errors that might occur when DIC is used outside of the window of a thermal chamber. They

concluded that the possible error in a temperature range between -45 °C to 85°C was negligible with values <1μm. Zhao et al. [36] also used a DIC setup for measurements within a temperature controlled chamber in order to obtain the CTE values of grade 45 steels, examining possible error factors as well. The results that they obtained matched the literature data, showing that image capturing with CCD cameras for DIC outside the window of a thermal chamber can provide accurate results.

Since there are currently few published experimental studies on adhesively bonded structures under thermal loading, further experimental research is necessary to address structural integrity issues in these assemblies. In this work, the aim was to achieve a clear understanding of the thermal/mechanical behaviour of multimaterial joints required to improve their design. DIC was employed to measure the displacement and the strain evolutions of the assemblies for temperatures in the range of 30°C to -40 °C in bonded assemblies of PMMA-glass with various bondline thicknesses. These two materials have significantly different CTE, which can make their joining problematic especially when stable performance is required in a wide temperature range of <-40 °C and up to 70 °C. A flexible elastomeric adhesive was selected as the joining medium, aiming to minimise the thermally induced strains in the bonded assembly. The experimental results are also compared against FEA results to give confidence in the DIC measurements, to help gain understanding of the underlying thermal/mechanical behaviour, and to show that FEA can be used to help improve the design of the bonded assemblies.

2 Materials and Test Methods

2.1 Sample fabrication

The bonded samples that were inspected with the use of DIC, were prepared with float glass (Quorn and Loughborough Glass, UK) and optical grade poly(methyl methacrylate) (PMMA) (Altuglas, Arkema, UK) adherends and using Sylgard ®184 (Dow Corning) a PDMS-based adhesive, as depicted in Figure 2. Prior to bonding, all samples were degreased with acetone using a lint-free cloth. Small acrylic spacers were inserted between the adherends to ensure a uniform bondline thickness. The spacers were placed near the middle of the samples in order not to affect the thermally induced strain field which is mainly focused towards the free ends of the samples. Masking tape was placed in the peripheral area of the bondline, to avoid any leakage due to the low

viscosity of the silicone adhesive. Sylgard® 184 was prepared by mixing the two parts in a 10:1 ratio according to the supplier's technical data sheet [37]. The adhesive was degassed prior to adhesion using a degassing chamber to eliminate the bubbles that were formed during the mixing of the two parts. The mixture was degassed 15 times under vacuum to 0.1 MPa over a total time of 20 minutes. The samples were left to cure at room temperature for 30 days prior to tensile testing. A total of three samples (S1, S2 and S3) were fabricated as indicated in Table 1.

Table 1: Characteristics of bonded samples used in the experimental investigation.

Sample number	Nominal adhesive thickness	Curing Times (days)	Area of interest	Test temp. range	Humidity
S1	0.5 mm	30	Narrow field	30°C to -40°C	0%
S2	2 mm	30	Narrow field	30°C to -40°C	0%
S3	3.2 mm	30	Narrow field	30°C to -40°C	0%

A matt-white background was applied with spray paint on the sides of the bonded samples. A single spray pass was applied in order not to produce a thick paint layer which could affect the micromovements of the samples' surface and not to be susceptible to cracking. Random black speckles were applied on top of the matt-white background to the sides of the samples using an Iwata-Custom Micron B airbrush and Tamiya acrylic paint. The paint was diluted with water (1 part:1 part water) before spraying. The air pressure was set to $4x10^5$ Pa, and the minimum nozzle size setting was used to for a small droplet size. The resulting speckle pattern is shown in Figure 3.

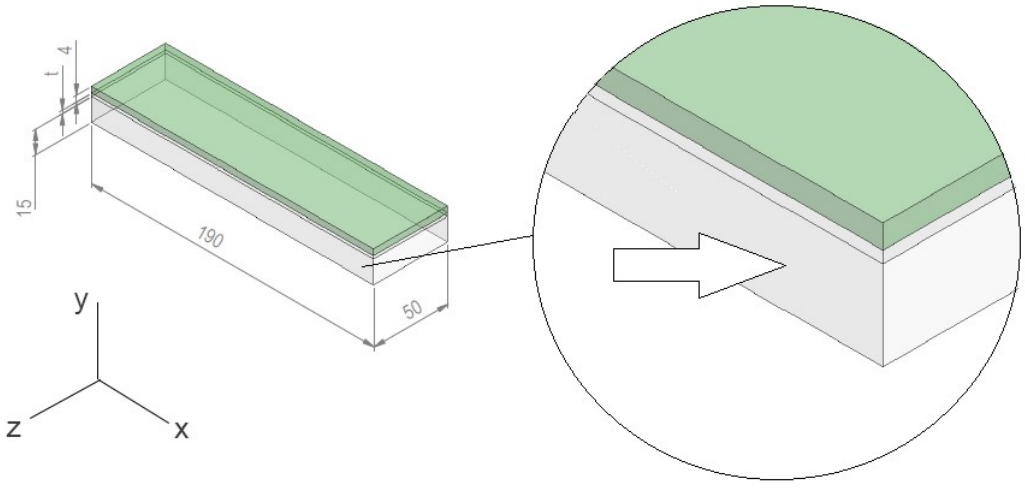

Figure 2: Bonded assembly and the area of interest of the narrow field DIC investigation. The three layers from top to bottom are the glass adherend, the PDMS adhesive in the middle and the PMMA substrate. With "t" is represented the variable thickness of the bond line. All units are in mm.

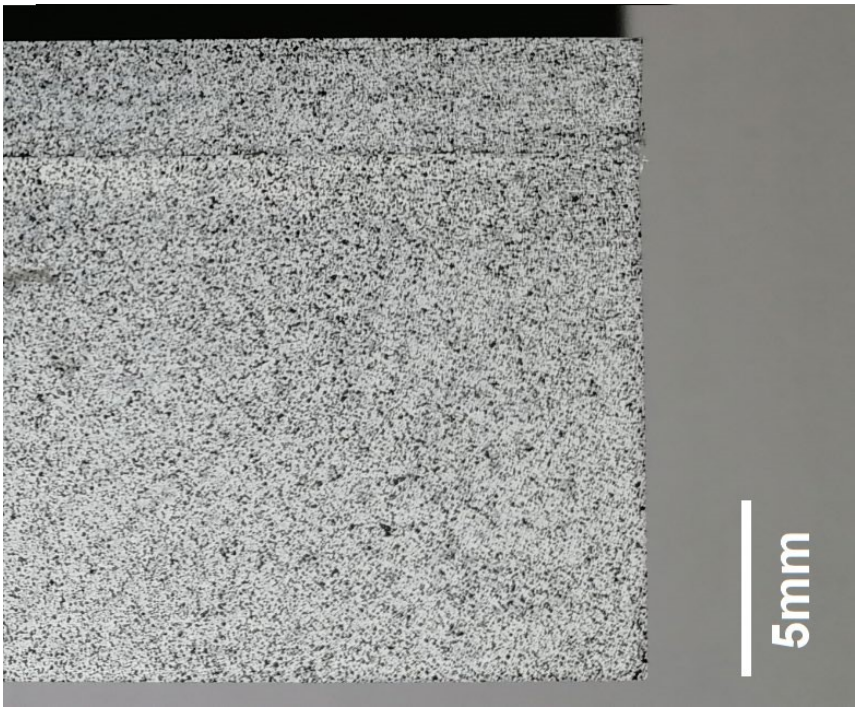

Figure 2: Typical speckle pattern in the edge of the bonded assembly.

2.2 Experimental test setup

The bonded samples were placed in an environmental chamber (WKL 34/70 Weiss Umwelttechnik, DE) with the area of interest facing towards the chamber window and the field view of the cameras. Controlled temperature (30 °C to -40 °C) and moisture (0%) conditions were used for the duration of the experiment. Three thermocouples were attached with adhesive tape, one on the right free edge of every layer of the assembly to ensure a uniform temperature during the measurements. The DIC strain data were captured at each 5°C interval.

To investigate the deformation of the bonded assemblies, a stereo 3D DIC camera system (LaVision GmbH, DE) was employed. The system consists of two Imager Elite cameras, each having a 1600×1200-pixel CCD arrays and 12-bit dynamic range), and each fitted with a Samyang 100-mm f/2.8 macro lens, as shown in Figure 4. A linear

LED illumination unit (with a white colour corresponding to 6500 K) was placed in front of the thermal chamber in such a way as to avoid the light reflection off the chamber's window, as shown in Figure 5. The system was calibrated before each experiment using a 3D calibration plate, (Type 106-10) with dimensions 106×106 mm supplied by the system manufacturer to correct possible lens distortions. In every calibration, the calibration plate was placed inside the chamber. The position and rotation of the two CCD cameras are presented in table 2. The speckled pattern on the assembly was recorded at a frequency of 1.5 Hz throughout the duration of each experiment and the DIC strain data were captured for 5 °C change steps with the Davis StrainMaster software (LaVision GmbH, DE). The specimen was allowed to achieve equilibrium at each temperature tested. For the post-processing of the captured images a region of interest (ROI) of 10×14 mm on the upper right corner of the assembly was selected with a mask and three seeding points were nominated within this region. A subset size of 24×24 pixels and a 5 pixel step size were used. The effect of subset size, step size, filtering and smoothing were tested before settling on the stated parameters. The surface displacements (u,v) of each recorded image was tracked relative to the initial image of the stress free assembly. The ε_{xx} , γ_{xy} , ε_{yy} strains fields were extracted from the displacement vector field [38]. The ε_{xx} , γ_{xy} are the strain values and describe the local one-dimensional deformation dL=L in x and y direction and γ_{xy} represent the local shear strain.

Table 2. Calibration fit parameters of the 2 CCD cameras

	Camera 1	**Camera 2**
Focal length	109 mm	109 mm
Distance in z	745.98 mm	741.6 mm
Rotation (x,y,z)	0°/12°/0°	0°/-12°/0°
St. Dev of fit	0.39	0.401

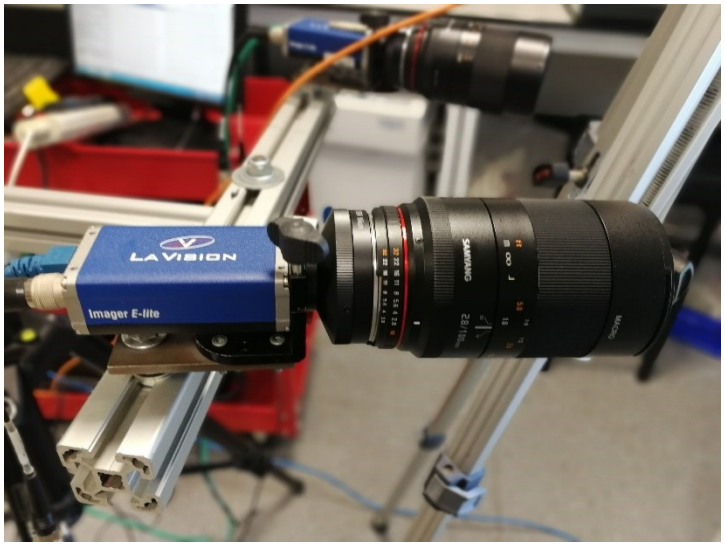

Figure 4: LaVision Imager E-lite camera with fitted Samyang 100mm f2.8 macro lens.

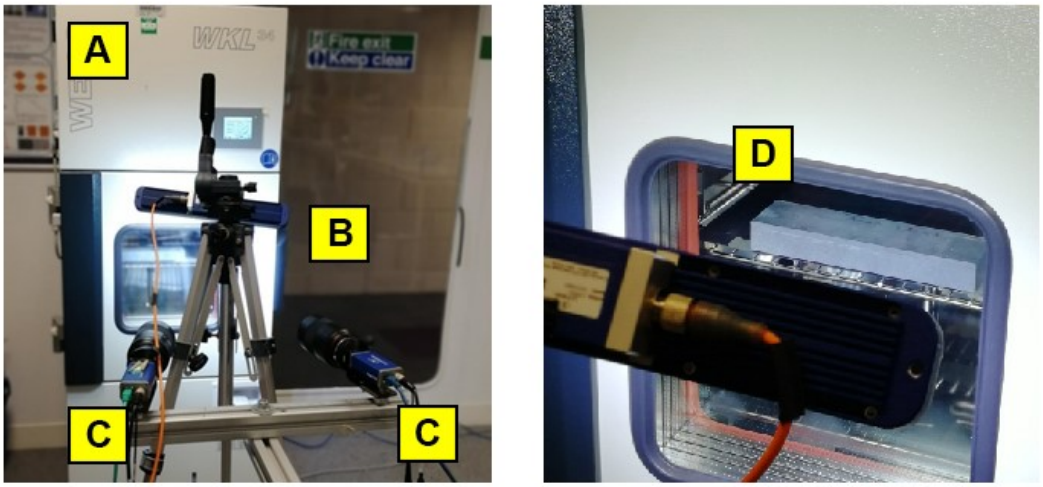

Figure 5: Digital image correlation setup with the controlled temperature chamber in which (A) is the controlled temperature chamber, (B) is the LED light source, (C) is the two CCD cameras, (D) is the test sample from a view inside the chamber through the chamber window.

3 FEA Stress Analysis

2D FEA was conducted by using the commercially available software package

COMSOL Multiphysics. With reference to Figure 6, the three layers from top to bottom are the glass adherend, the PDMS adhesive in the middle and the PMMA substrate. Due to the symmetrical geometry of the bonded specimens, only half of the bonded assembly was modelled: A symmetric boundary was employed on the left edge of the assembly; the remaining edges are free. A rigid motion suppression point was fixed in the middle of the left edge of the bondline to eliminate the rigid displacements but to allow the free deformation of the assembly. Displacement boundary conditions were applied to the rest of the nodes. A static, linear material model was employed, and a linear solver was used.

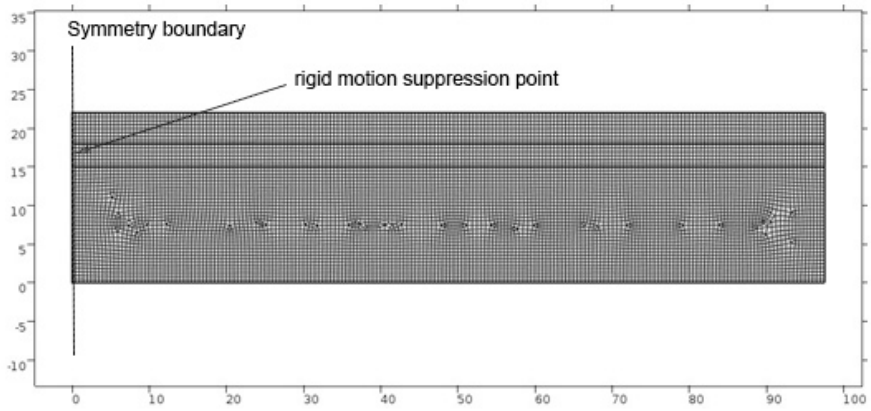

Figure 6: Mesh of the bonded assembly. The mesh across the thickness of the adhesive consists of 6 elements. All units are in mm.

A mesh convergence study was performed to determine the appropriate mesh refinement size, which indicated the use of minimum of six elements across the thickness of the adhesive. The selected mesh comprises 9089 quadratic elements with minimum element quality 0.5; see Figure 6. A 2D model was employed to simulate the behaviour of the bonded assembly with a bondline thickness of 2 mm, in a homogeneous temperature field of -30 °C, since at this temperature the maximum strains were observed with DIC prior to the failure of the PMMA-PDMS interface. Since the strain

distribution is examined only on the external surfaces, a 2D study is considered adequate. PDMS has a linear elastic behaviour in strain levels less than 40% [39,40] and due to the fact that significantly lower (<<40%) strain values were observed in the experimental investigation, all three layers are modelled as isotropic and linear elastic. At higher strains, PDMS displays hyperelastic behaviour and non-linear elastic material models such as Neo-Hookean, Mooney–Rivlin and Ogden would become necessary [41,42]. Since the polymeric materials have temperature-dependent mechanical properties, the Young's modulus and coefficient of thermal expansion values of PMMA and PDMS were selected at the temperature of -30 °C [43–45]. The mechanical properties of the glass adherend were considered constant in the specific temperature range. A multipoint constraint algorithm was employed to ensure a perfect bonding between the glass/adhesive and PMMA/adhesive interfaces. The material properties used for the simulation are given in Table 3. Material properties of Sylgard® 184 were obtained from [46].

Table 3: Material properties of glass, Sylgard® 184 and PMMA at 30 °C and -30 °C.

		Glass	Sylgard® 184 at 30 °C	PMMA at 30 °C	Sylgard® 184 at -30 °C	PMMA at -30 °C
Coefficient of thermal expansion [K^{-1}]	α	8.3×10^{-6}	3.2×10^{-5}	7×10^{-5}	3.2×10^{-5}	7×10^{-5}
Young's modulus [Pa]	E	70×10^{9}	1.32×10^{6}	3.2×10^{9}	1.95×10^{6}	4.3×10^{9}
Poisson ratio	ν	0.25	0.499	0.35	0.499	0.35

4 Results and discussion

4.1 In-plane displacement contours

The DIC measurement of displacements u and v along the x- and y-axes of the assembly at -30° C are shown in Figures 7 and 8. The figures refer to the upper right corner of the bonded assembly; see Figure 2, with the area shown measuring 10×14 mm. As expected, due to the different CTEs of the three layers, there is a bigger contraction of the PMMA substrate compared to the glass adherend in this region. The flexible silicone layer is compensating this difference by being able to deform unevenly with smaller

contraction at the top of the bondline and larger towards the PMMA substrate. A high deformation is also observed at the middle of the free edge of the silicone layer since it is not as constrained as it is at the two interfaces of the assembly. The v displacement in y direction as shown in Figure 8, can reveal the bending that occurs in the structure due to the CTE mismatch of the substrates and the change of curvature of the assembly. A higher displacement is observed towards the upper right edge of the assembly which is decreasing towards the centre. Similarly, in this case, the flexible adhesive layer compensates the different displacement of the substrates.

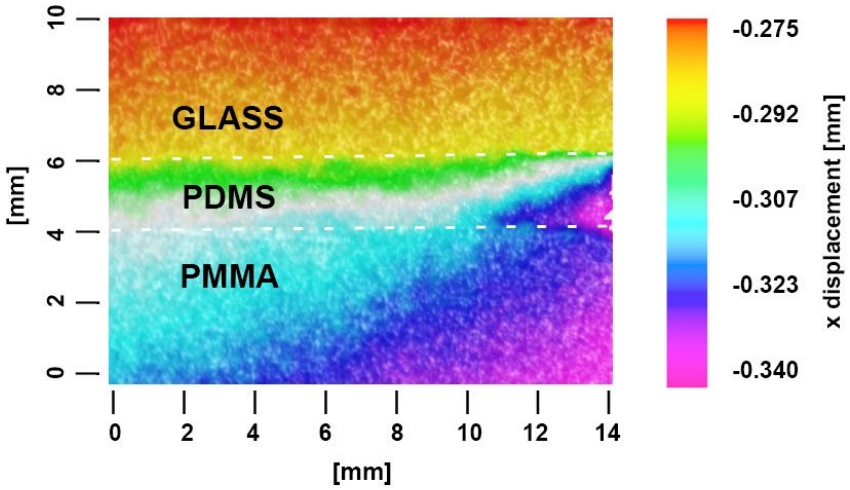

Figure 7: Displacements in u (x direction) of the bonded assembly with an adhesive thickness of 2 mm in a chamber temperature of -30° C.

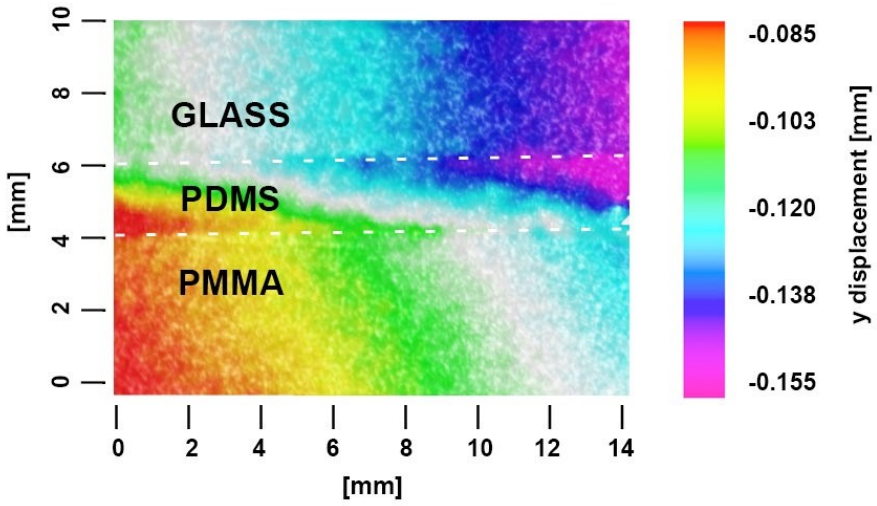

Figure 8: Displacements in v (y direction) of the bonded assembly with an adhesive thickness of 2 mm in a chamber temperature of -30° C.

4.2 Longitudinal, transverse and shear strain distribution

Figures 9, 10 and 11 represent the development of the longitudinal, shear and transverse strains respectively, in the assembly with 2 mm adhesive thickness at different times and so temperatures, these being 0 °C, -15 °C, -30 °C, -40 °C. The longitudinal strains (ε_{xx}) start to develop near the free edge of the bondline reaching a value of -0.028 before the initiation of the delamination. The development of the shear strains (γ_{xy}) is observed at the two interfaces of the assembly near the free edge. The dissimilarity of the materials' CTE leads to bigger contraction of the PMMA substrate compared to glass, as is also observed in their displacements in x and y directions, and as a result positive strains appears at the glass-silicone interface and a concentration of negative strains at the PMMA-silicone interface towards the free edge. Over time the positive strain dominates in the bondline, expanding up to 10 mm towards the centre of the assembly and the negative strain is concentrated at the point of the PMMA-silicone interface which is located next to the free edge of the assembly. The maximum shear strain before failure is 0.036. The peeling (transverse) strain (ε_{yy}) development is depicted in Figure 4.11. It mainly starts to develop at the interfaces and over the further decrease of the temperature it is also transferred all over the thickness of the assembly. It is observed

that a positive strain is developed in the glass-silicone interface and a negative strain dominates in the PMMA-silicone interface. The bonded structure is contracting together as a system but also every layer is subjected to a lateral and longitudinal contraction separately as well. The dissimilar contraction of the layers of the structure leads to the development of a positive transverse strain at the glass-silicone interface reaching a maximum value of 0.05. A similar behaviour is also observed in the biggest part of PMMA-silicone interface reaching a value of -0.045. Although, towards the free edge of the PMMA-silicone interface; see Figure 11(c), there is a small concentration of a positive transverse strain with a value of 0.05 before the delamination is initiated. The transverse strain in the middle of the assembly reaches an average value of -0.02. In every case, strains of negligible value appear at the two unconstrained substrates apart of their interfaces with the adhesive layer.

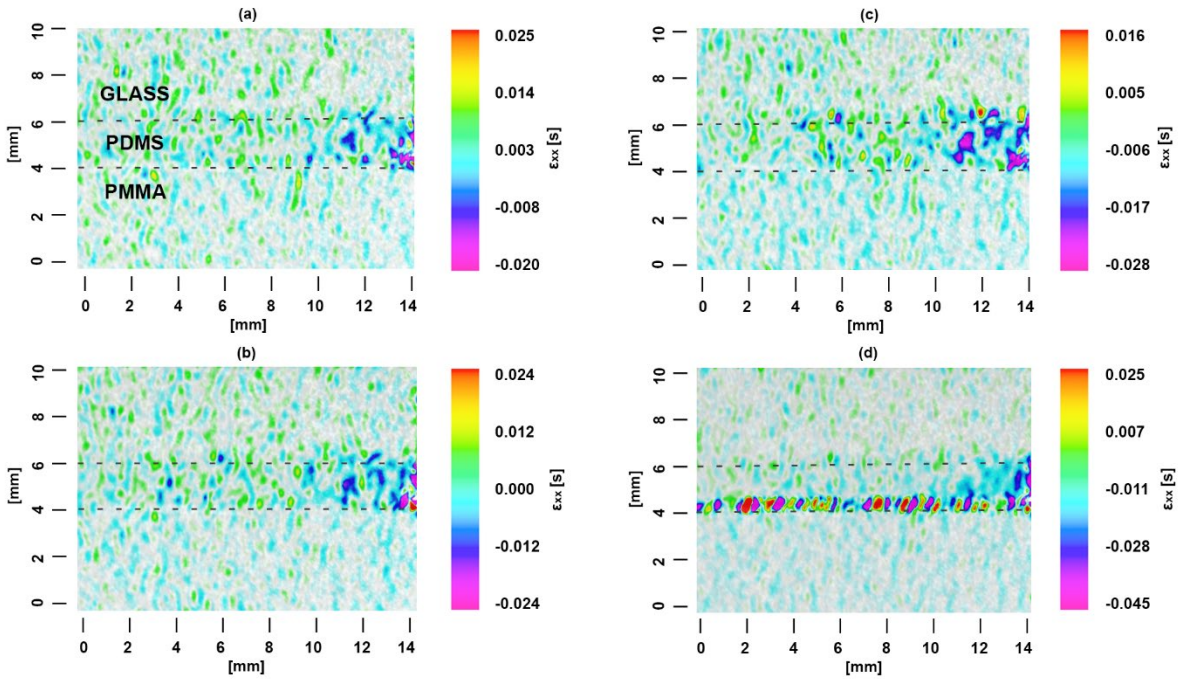

Figure 9: Tensile strain (ε_{xx}) development and failure via delamination in trilayer assembly (Glass-PDMS-PMMA) due to CTE mismatch in 0 °C (a), -15 °C (b), -30 °C (c), -40 °C (d).

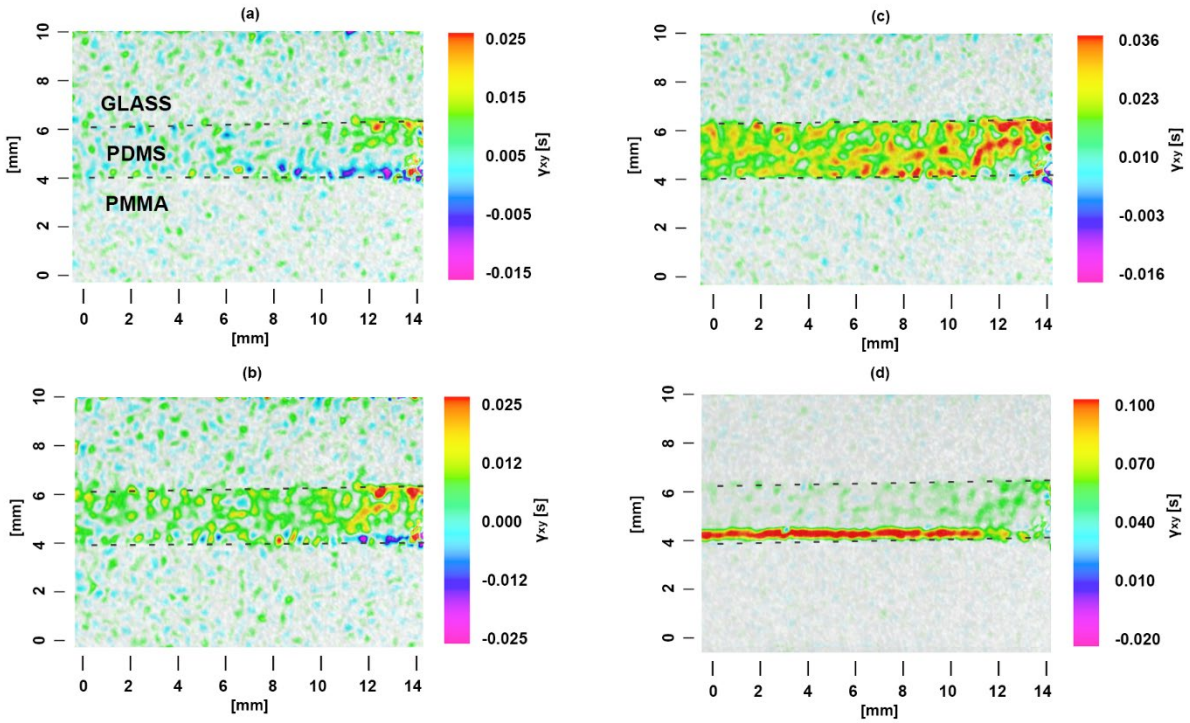

Figure 10: Shear strain (γ_{xy}) development and failure via delamination in trilayer assembly (Glass-PDMS-PMMA) due to CTE mismatch in 0 °C (a), -15 °C (b), -30 °C(c),-40°C(d).

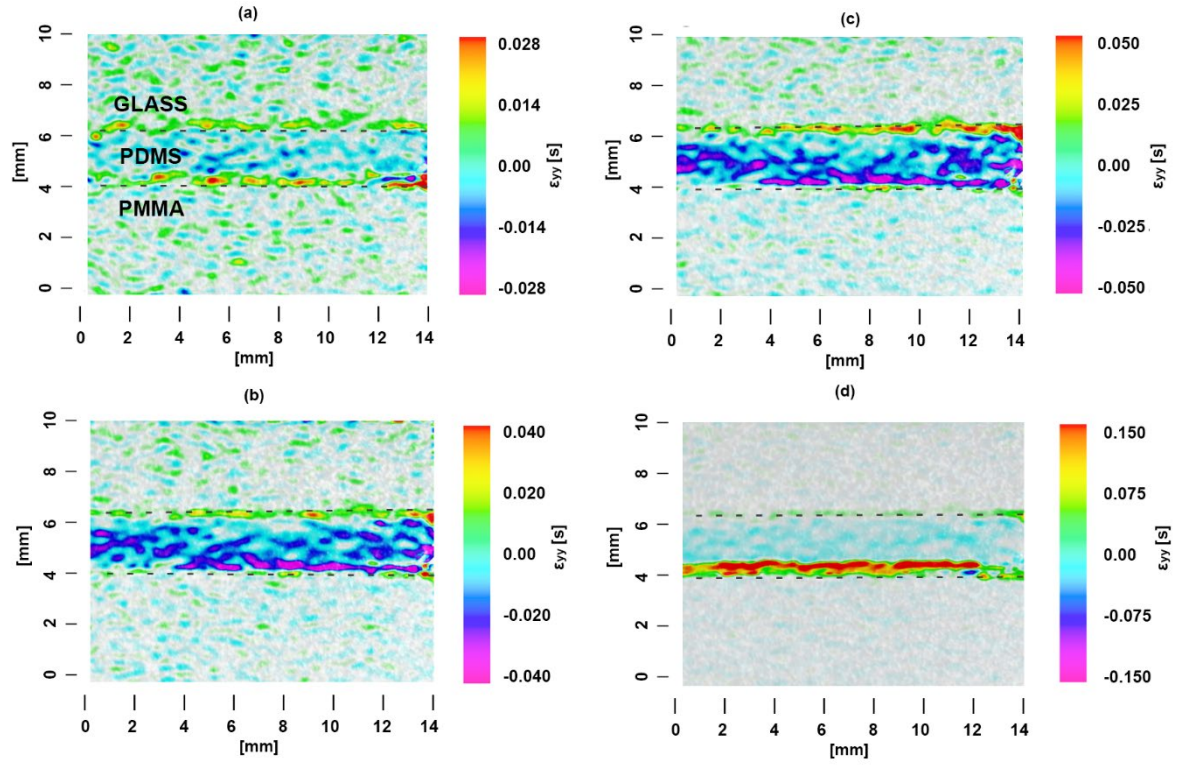

Figure 11. Peeling strain (ε_{yy}) development and failure via delamination in trilayer assembly (Glass-PDMS-PMMA) due to CTE mismatch in 0 °C (a), -15 °C (b), -30 °C (c), -40 °C (d).

4.3 Strain development within the adhesive layer for variable bondline thicknesses

Figures 13, 14 and 15 represent the development of the longitudinal (ε_{xx}), transverse (ε_{yy}) and shear (γ_{xy}) strains in the middle of the adhesive layer, 0.5 mm away from the free edge of the assembly, as depicted in Figure 12, as a function of temperature for assemblies with bondline thicknesses of 0.5, 2.0 and 3.2 mm respectively. With the continuous inspection of the bonded assembly with DIC, it is possible to determine accurately the temperature and strain values where the failure of the joint initiates. In the present case, this occurs via delamination at the PMMA-to-silicone interface.

In the present experiments, the assembly bonded with a silicone adhesive with a thickness of 0.5 mm started to fail after the temperature reached ~-20°C inside the thermal chamber, the assembly with 2 mm adhesive thickness close to a temperature of ~-30°C and the assembly with 3.2 mm adhesive thickness remained undamaged during the course of the experiment (<-40°C). It is observed that the strains in the joints with thinner adhesive bondlines are developed more rapidly and subsequently they tend to fail earlier than the joints with thicker bondlines. For example, at a temperature of 20°C, the shear strain is 0.027, 0.021 and 0.016 for bondline thicknesses of 0.5, 2 and 3.2 mm respectively. Similarly, the transverse strains at the same moment are 0.039, 0.32 and 0.026. From the experiments, it becomes clear that the transverse (peeling) strains have the biggest absolute magnitude followed by the shear and the longitudinal strains appear to have the weakest development in the bond line. For the assembly with the thickest bondline (3.2 mm) that remained intact after exposure to -40°C, the developed strains are ε_{yy}=-0.056, γ_{xy}=0.049 and ε_{xx}=-0.018. From the above observations it can be assumed that thicker bondlines of flexible adhesives in assemblies with materials with significantly different CTEs exposed to low temperatures, can accommodate more efficiently the dissimilar contractions of the substrates and are capable to withstand the thermally induced strains.

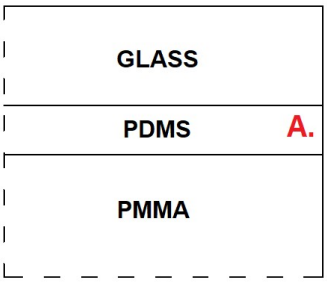

Figure 12: Data acquisition point (A) for the strain development in the middle the bondline near the free edge of the assembly (0.5mm).

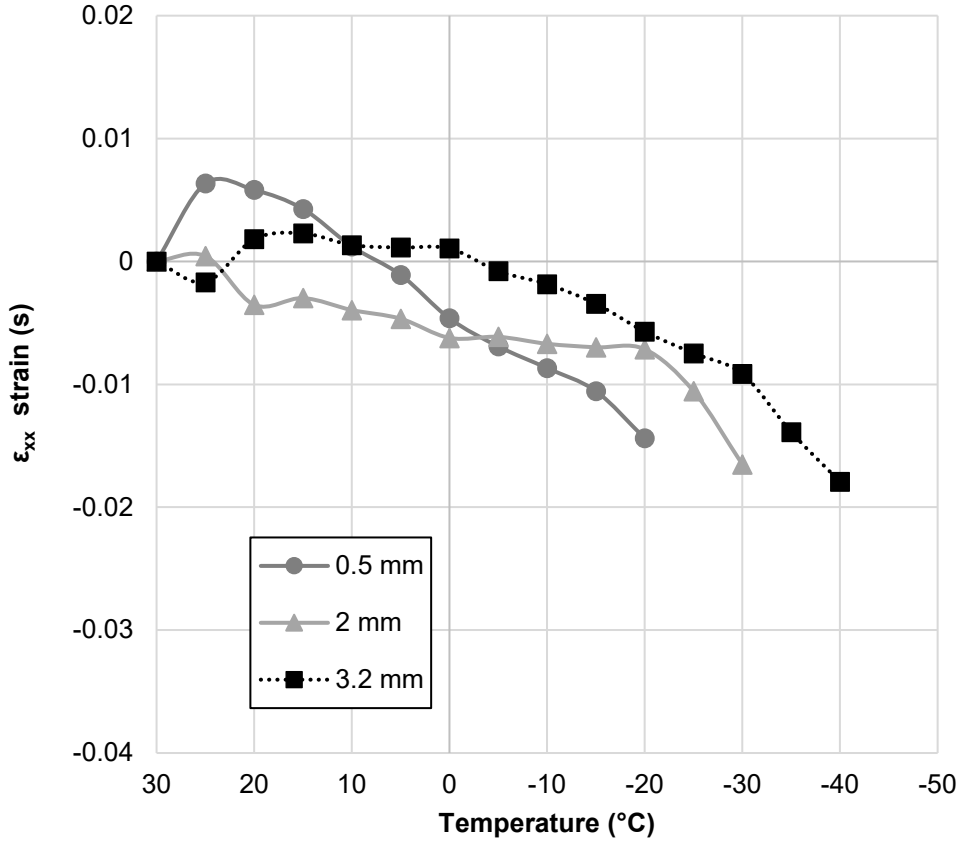

Figure 13: Plot of ε_{xx} strain development over temperature within the bondline next to the free edge of the glass-PMMA assembly bonded with PDMS adhesive with thickness of 0.5, 2, 3.2 mm.

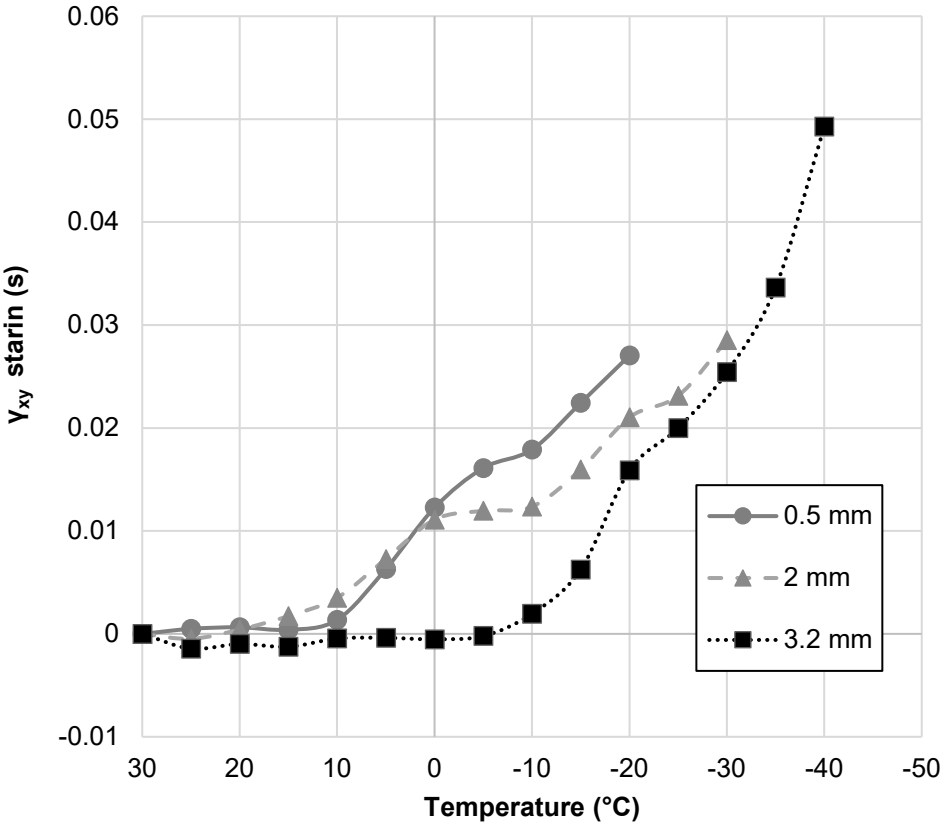

Figure 14: Plot of γ_{xy} strain development over temperature within the bondline next to the free edge of the glass-PMMA assembly bonded with PDMS adhesive with thickness of 0.5, 2, 3.2 mm.

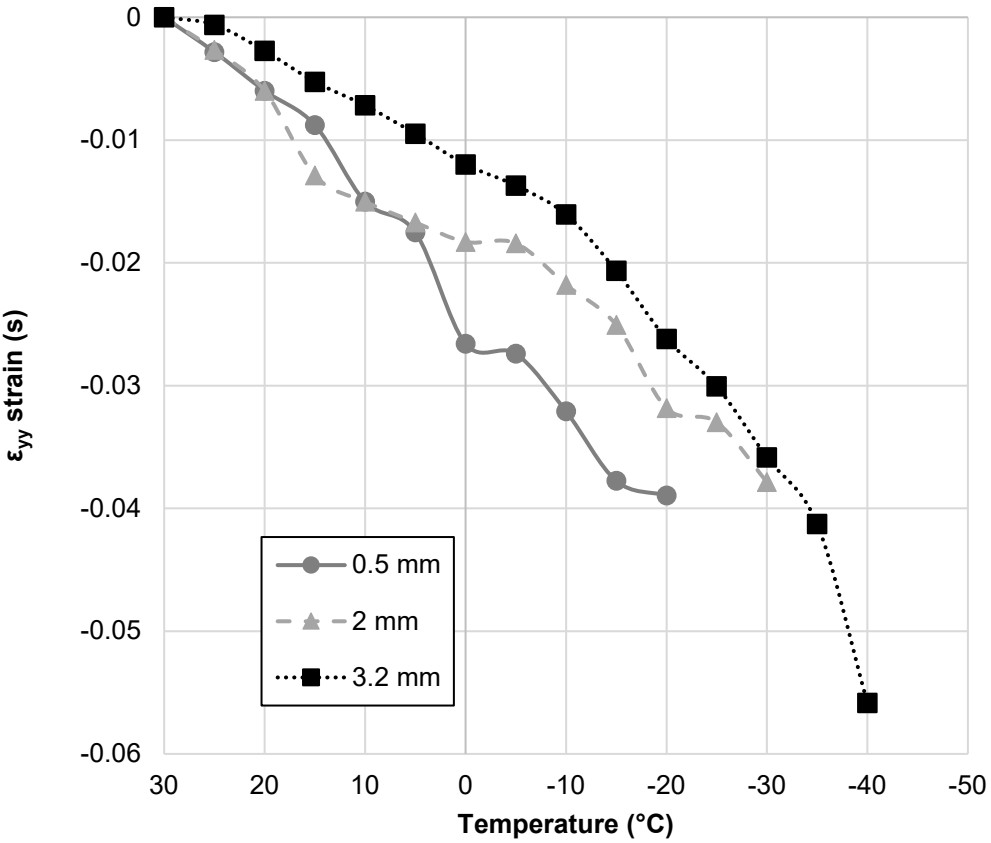

Figure 15: Plot of ε_{yy} strain development over temperature within the bondline next to the free edge of the glass-PMMA assembly bonded with PDMS adhesive with thickness of 0.5, 2, 3.2 mm.

4.4 Comparison of experimental results with finite element analysis results

To assess the accuracy of the present experiment, the results are compared with those obtained by FEA. Figures 17, 18 and 19 present comparative plots of the results acquired from the experimental investigation with DIC and the results of the FE model at -30 °C. The plots represent the averaged strain distribution 0.1 mm away from the edge of the assembly across the B-B' line as depicted in Figure 16.

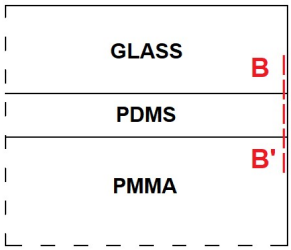

Figure 16: Data acquisition line (B-B') for the strain distribution next to the free edge of the bonded assembly (0.1mm).

From figures 17 to 19, it can be seen that good agreement is observed between the experimental and the FEA results with a similar strain distribution indicated across the three layers. In the longitudinal strain distribution, there is an identical fitting between the two results in the PMMA-PDMS interface. Also, analogous behaviour is observed near the PDMS-glass interface with similar strain peaks at 0.1 mm from the edge of the assembly where the strain values are 0.038 and 0.039 for the FEA and the DIC results respectively. In the shear strain distribution, a difference of less than 1% between the strain values is detected at the two interfaces. Similarly, for the peeling strain distribution, there is a good agreement between the experimental and numerical results at the two interfaces. The main anomaly is detected in the middle section of the bondline which can be possibly be attributed to errors in the calculated FEA model due to its two dimensional hypostasis.

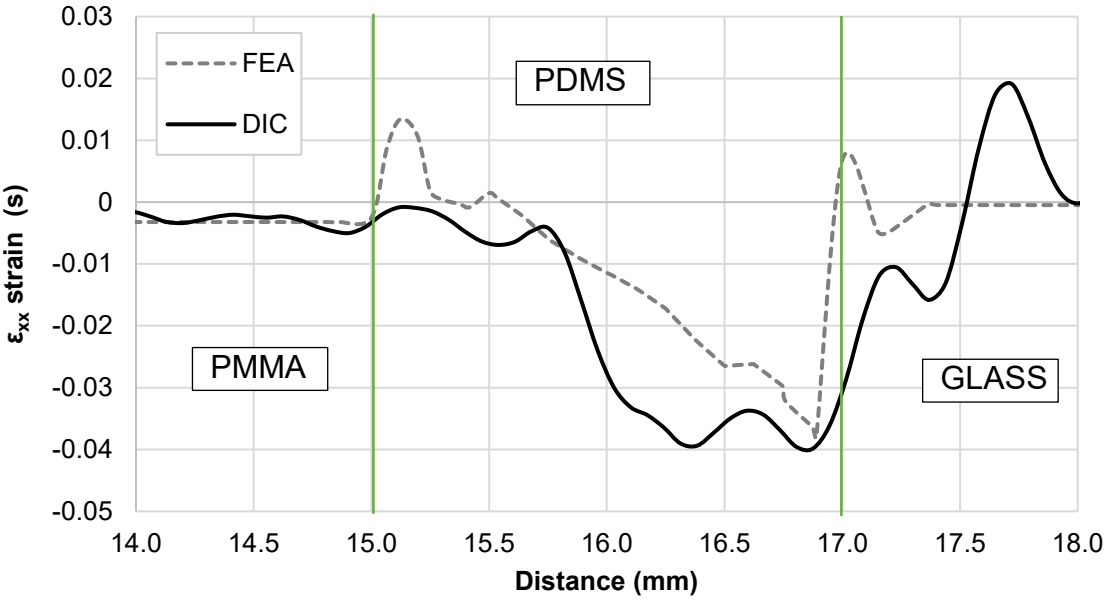

Figure 17: Comparative plot of ε_{xx} strain distribution in the PDMS adhesive layer with 2 mm thickness between PMMA substrate and glass adherend obtained from DIC and FEA results at -30 °C.

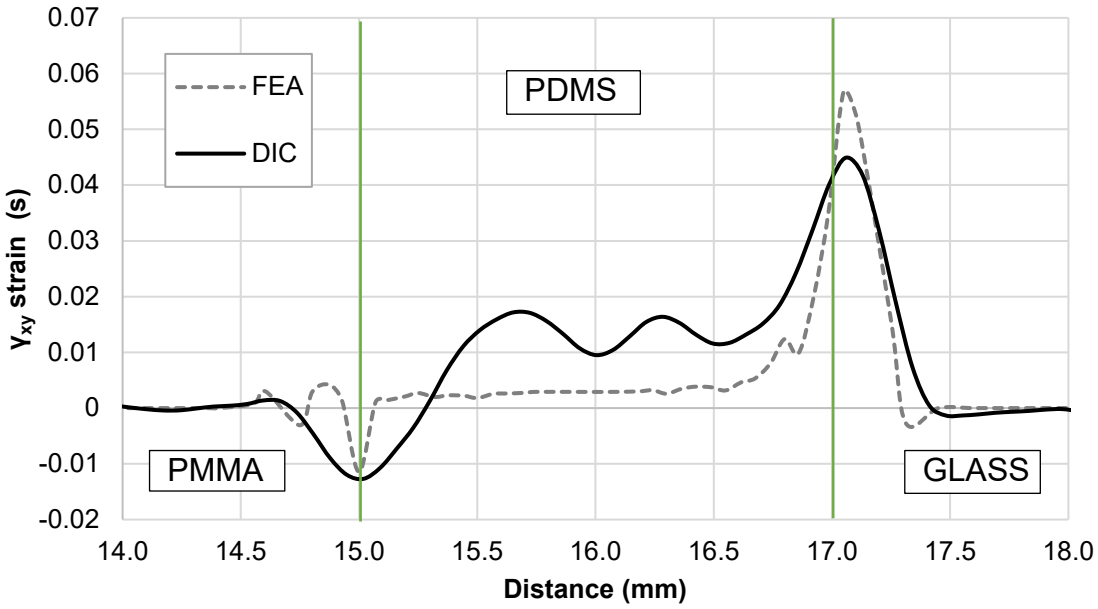

Figure 18: Comparative plot of γ_{xy} strain distribution in the PDMS adhesive layer with 2 mm thickness between PMMA substrate and glass adherend obtained from DIC and FEA results at -30 °C.

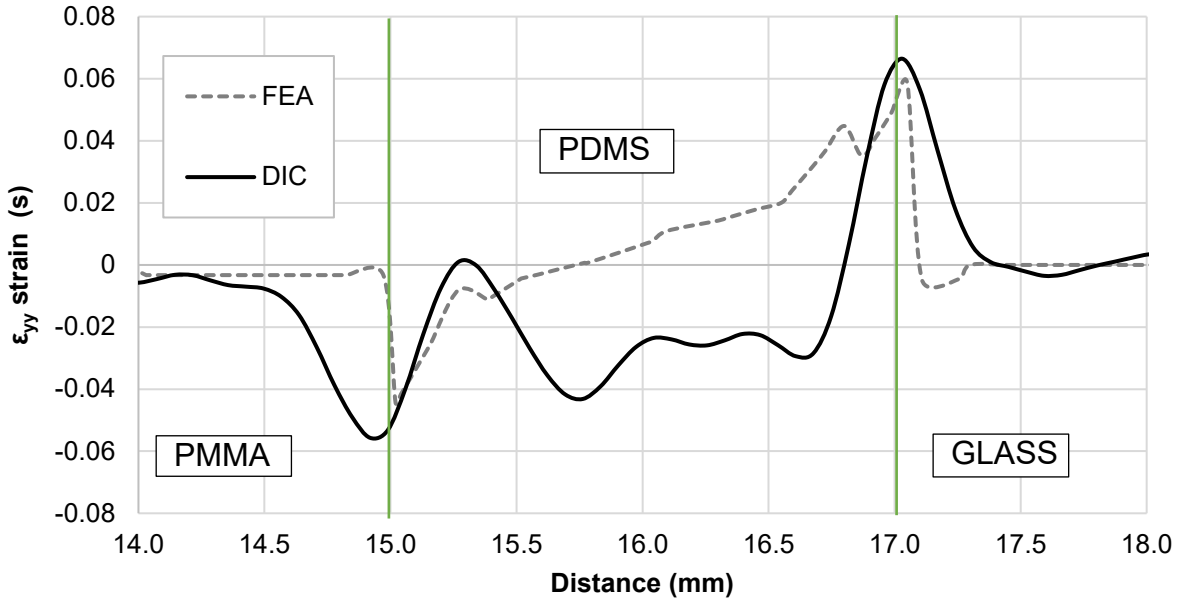

Figure 19: Comparative plot of ε_{yy} strain distribution in the PDMS adhesive layer with 2 mm thickness between PMMA substrate and glass adherend obtained from DIC and FEA results at -30 °C.

5 Conclusions

- The aim of the present study was to evaluate the differential strains that develop in bonded joints at low temperatures using an experimental technique, namely DIC.

- To achieve this, recording of the behaviour of bonded assemblies, incorporating PMMA and glass adherends and a flexible PDMS-based adhesive, was captured with a stereo 3D DIC camera system through the window of a temperature-controlled chamber.

- Specimens with different bondline thicknesses were produced to investigate the effect of the adhesive thickness in the developed strains. The investigation of the developed strain field due to the temperature change can provide a better understanding of the load transfer, the strain concentration areas and the damage initiation mechanisms. A better

understanding can lead consequently to optimized joint design and selection of appropriate surface treatments for the enhancement of the joints' strength.

- It is concluded that, the proposed experimental test setup with the employment of the DIC technique can successfully indicate the displacement contours in bonded joints exposed to temperature gradients.

- Additionally, the conversion of the displacements to strain maps, captures the developed strains in the adherends and through the thickness of the adhesive layers. Also, the continuous monitoring of the bonded assemblies in different temperatures may provide the conditions (temperature and developed strains) at the moment of failure.

- It was also observed that a more rapid strain development appears when thinner bondlines were employed compared to thicker ones. As a result, earlier failures in higher temperatures were observed for the assemblies bonded with thinner bondlines whereas thicker bondlines accommodated more efficiently the thermally induced strains. The developed transverse (peeling) strains appeared to have the largest values through the thickness of the bondline. Shear and even more longitudinal strains appeared to have the weakest development within the bond line.

- Good agreement was observed comparing the DIC results with those acquired from a 2D FEA model, indicating that DIC can be a highly reliable method for the monitoring of thermally induced strains in bonded assemblies.

- Overall, the investigation of the developed strain field, using the DIC method, as a function of temperature changes can provide a better understanding of: adherend deformations; the strain concentration areas, and; the damage initiation mechanisms.

6 References

[1] Mai E-HW and Y-W. Robust Design of Microelectronics Assemblies Against Mechanical Shock, Temperature and Moisture. 2016. doi:10.1016/c2013-017253-4.

[2] Turner PS. The problem of thermal-expansion stresses in reinforced plastics. Natl Advis Committes Aeronaut 1942;36:1–23. doi:10.1177/0162243907306194.

[3] Adams RD, Coppendale J, Mallick V, Al-Hamdan H. The effect of temperature on the strength of adhesive joints. Int J Adhes Adhes 1992;12:185–90. doi:10.1016/0143-7496(92)90052-W.

[4] Dong CY, Lee KY. Stress analysis of plastic IC package containing various interface delaminations using the boundary element method. Eng Fract Mech 2008;75:1–16. doi:10.1016/j.engfracmech.2007.03.019.

[5] Suhir E. Thermal stress failures in electronics and photonics: Physics, modeling, prevention. J Therm Stress 2013;36:537–63. doi:10.1080/01495739.2013.784119.

[6] Hatheway AE. Designing elastomeric mirror mountings. New Dev Optomech 2007;6665:666504. doi:10.1117/12.740025.

[7] Down JL, MacDonald MA, Tétreault J, Williams RS, Tetreault J. Adhesive Testing at the Canadian Conservation Institute: An Evaluation of Selected Poly(Vinyl Acetate) and Acrylic Adhesives. Stud Conserv 2006;41:19. doi:10.2307/1506550.

[8] Susan Levandoski JoAnn DeMarco. Non-yellowing fast cure speed UV\visible curable liquid acrylic ester adhesives for glass bonding 2001;1.

[9] Kim K, Park SW, Yang SS. The optimization of PDMS-PMMA bonding process using silane primer. Biochip J 2010;4:148–54. doi:10.1007/s13206-010-4210-0.

[10] V.Bagiatis, Critchlow GW, Price D, Wang S. The effect of atmospheric pressure plasma treatment (APPT) on the adhesive bonding of poly(methyl methacrylate) (PMMA)-to-glass using a polydimethylsiloxane (PDMS)-based adhesive. Int J Adhes Adhes 2019:102405. doi:10.1016/j.ijadhadh.2019.102405.

[11] Da Silva LFM, Adams RD. Stress-free temperature in a mixed-adhesive joint. J Adhes Sci Technol 2006;20:1705–26. doi:10.1163/156856106779024436.

[12] Taylor TC, Yuan FL. Thermal Stress and Fracture in Shear-Constrained Semiconductor Device Structures. IRE Trans Electron Devices 1962;9:303–8. doi:10.1109/T-ED.1962.14987.

[13] Volkersen O. Die nietkraftverteilung in zugbeanspruchten mit konstanten laschenquerschritten. Luftfahrtforschung 1938;15:41–7.

[14] Chen, W. T., & Nelson CW. Thermal Stress in Bonded Joints. IBM J Res Dev 1979;23:178–88.

[15] Suhir E. Stresses in bi-metal thermostats. ASME J Appl Mech 1986;53:657–60.

[16] Suhir E. An Approximate Analysis of Stresses in Multilayered Elastic Thin Films. J Appl Mech 1988;55:143. doi:10.1115/1.3173620.

[17] Suhir E. Thermal stress failures in microelectronic components - review and extension. Adv Therm Model Electron Components Syst 1988.

[18] Jiang ZQ, Huang Y, Chandra A. Thermal Stresses in Layered Electronic Assemblies. J Electron Packag 1997;119:127–32. doi:10.1115/1.2792218.

[19] Wong EH, Lim KM, Mai YW. Analytical solutions for PCB assembly subjected to mismatched thermal expansion. IEEE Trans Adv Packag 2009;32:602–11. doi:10.1109/TADVP.2009.2025222.

[20] He J, Zhou W, He X, Yu H, Peng P, Wang S. Analytical model for adhesive dieattaching subjected to thermal loads using second-order beam theory. Int J Adhes Adhes 2018;82:282–9. doi:10.1016/j.ijadhadh.2018.01.016.

[21] Moutrille MP, Derrien K, Baptiste D, Balandraud X, Grédiac M. Throughthickness strain field measurement in a composite/aluminium adhesive joint.
Compos Part A Appl Sci Manuf 2009;40:985–96. doi:10.1016/j.compositesa.2008.04.018.

[22] Kashfuddoja M, Ramji M. Assessment of local strain field in adhesive layer of an unsymmetrically repaired CFRP panel using digital image correlation. Int J Adhes Adhes 2015;57:57–69. doi:10.1016/j.ijadhadh.2014.10.005.

[23] Kosmann J, Völkerink O, Schollerer MJ, Holzhüter D, Hühne C. Digital image correlation strain measurement of thick adherend shear test specimen joined with an epoxy film adhesive. Int J Adhes Adhes 2019;90:32–7. doi:10.1016/j.ijadhadh.2019.01.024.

[24] R J, Naik GN. Single and dual adhesive bond strength analysis of single lap joint between dissimilar adherends. Int J Adhes Adhes 2019;92:142–53. doi:10.1016/j.ijadhadh.2019.04.016.

[25] Bamberg PAMGP, Reisgen U, Schiebahn A, Barbosa JDV, Marx B, Coelho RS. Digital Image Correlation Analysis Of The Effects Of The Overlap Length, Adhesive Thickness And Adherends Yield Strength Over Similar And Dissimilar Joints Of High Strength Steel And Aluminum Alloys. Int J Adhes Adhes 2018;83:69–75. doi:10.1016/j.ijadhadh.2018.02.010.

[26] Caminero MA, Lopez-Pedrosa M, Pinna C, Soutis C. Damage monitoring and analysis of composite laminates with an open hole and adhesively bonded repairs using digital image correlation. Compos Part B Eng 2013;53:76–91. doi:10.1016/j.compositesb.2013.04.050.

[27] Silva TC, Nunes LCS. A new experimental approach for the estimation of bending moments in adhesively bonded single lap joints. Int J Adhes Adhes 2014;54:13–20. doi:10.1016/j.ijadhadh.2014.04.006.

[28] Bai R, Bao S, Lei Z, Yan C, Han X. Finite element inversion method for interfacial stress analysis of composite single-lap adhesively bonded joint based on full-field deformation. Int J Adhes Adhes 2018;81:48–55. doi:10.1016/j.ijadhadh.2017.11.011.

[29] Crammond G, Boyd SW, Dulieu-Barton JM. Evaluating the localised throughthickness load transfer and damage initiation in a composite joint using digital image correlation. Compos Part A Appl Sci Manuf 2014;61:224–34. doi:10.1016/j.compositesa.2014.03.002.

[30] Zarouchas D, Van Hemelrijck D. Mechanical characterization and damage assessment of thick adhesives for wind turbine blades using acoustic emission and digital image correlation techniques. J Adhes Sci Technol 2014;28:1500–16. doi:10.1080/01694243.2012.698122.

[31] Kwak J. Strain behaviors of solder bump with underfill for flip chip package under thermal loading condition. J Mech Sci Technol 2014;28:4899–906. doi:10.1007/s12206-014-1109-z.

[32] Yoshida HJ• CS• S, Lamberti L. Advancement of Optical Methods in Experimental Mechanics, Volume 3 Conference Proceedings of the Society for Experimental Mechanics Series. vol. 3. n.d.

[33] Zhang, J., Li, M., Xiong, C., Fang, J., & Yi, S.H. (2005). Thermal deformation analysis of BGA package by digital image correlation technique. n.d.

[34] Deheeger A, Badulescu C, Mathias JD, Grédiac M. Experimental study of thermal stresses in a bonded joint. J Phys Conf Ser 2009;181. doi:10.1088/17426596/181/1/012041.

[35] Eitner U, Köntges M, Brendel R. Use of digital image correlation technique to determine thermomechanical deformations in photovoltaic laminates: Measurements and accuracy. Sol Energy Mater Sol Cells 2010;94:1346–51. doi:10.1016/j.solmat.2010.03.028.

[36] Jian Z, Dong Z, Zhe Z. A Non-Contact Varying Temperature Strain Measuring System Based on Digital Image Correlation. Exp Tech 2016;40:101–10. doi:10.1007/s40799-016-0014-z.

[37] Dow Chemical Company T. SYLGARD^{TM} 184 Silicone Elastomer FEATURES & BENEFITS 2017.

[38] LaVision GmbH. StrainMaster LaVision. 2012.

[39] Schneider F, Fellner T, Wilde J, Wallrabe U. Mechanical properties of silicones for MEMS. J Micromechanics Microengineering 2008;18. doi:10.1088/09601317/18/6/065008.

[40] Johnston ID, McCluskey DK, Tan CKL, Tracey MC. Mechanical characterization of bulk Sylgard 184 for microfluidics and microengineering. J Micromechanics Microengineering 2014;24. doi:10.1088/0960-1317/24/3/035017.

[41] Kim TK, Kim JK, Jeong OC. Measurement of nonlinear mechanical properties of PDMS elastomer. Microelectron Eng 2011;88:1982–5. doi:10.1016/j.mee.2010.12.108.

[42] Schaap A, Bellouard Y. Molding topologically-complex 3D polymer microstructures from femtosecond laser machined glass. Opt Mater Express 2013;3:1428. doi:10.1364/ome.3.001428.

[43] Physical S, Of TP. Selected Physical and Thermal Properties of Various Formulations of Silicone Potting Compounds n.d.

[44] Geoffrey K. Thermal expansion of glasses at low temperatures. Retrosp Theses Diss 1978:6571.

[45] Sahputra IH, Alexiadis A, Adams MJ. Temperature dependence of the Young's modulus of polymers calculated using a hybrid molecular mechanics-molecular dynamics method. J Phys Condens Matter 2018;30. doi:10.1088/1361648X/aad588.

[46] Sylgard 184: shear modulus vs temp n.d. https://www.sandia.gov/polymerproperties/E1-G_vs_temp.html (accessed March 26, 2020).